Integral Representation of Spatial Green's Function and Spectral Domain Analysis of Leaky Covered Strip-Like Lines

Francisco Mesa and Ricardo Marqués

Abstract—**This paper studies the possible integral representations of the Spatial Dyadic Green's Function of a laterally open but covered multilayered planar waveguide with translation symmetry. Among all of integral representations, we especially focus on that unique representation which comprises only outgoing waves (energy transferred from the source to infinity in case lateral radiation was present). We propose this specific integral representation as the most appropriate in the Spectral Domain Analysis of strip-like structures when these are assumed to be guiding/leaky systems with translation symmetry. This integral representation directly provides the integration contour to be used in the definition of the inverse Fourier transform. Some aspects concerning the use of the nonconventional Fourier transform are discussed in connection with the application of the Method of Moments. It is also highlighted that the dispersion relation of the strip-like configuration is expressed in terms of the zeros of a multivalued complex function. This fact becomes relevant when searching for zeros out of the spectral sheet (i.e., zeros associated with leaky modes). Finally, some numerical results are presented. These computed values show good agreement when compared with some previously published data. The influence of different definitions of the inverse integration contour on the propagation characteristics of a pair of coplanar coupled strips is also investigated. Computed data will show the leakage characteristics of a pair of noncoplanar strips.**

I. Introduction

THE ANALYSIS of electromagnetic propagation in laterally unbounded planar layered structures with top and bottom impenetrable walls is treated once again in connection with the leakage phenomenon. Many examples can be found in the literature dealing with this topic, i.e., [1]–[3]. Two different approaches have been used to analyze the leaky regime: mode-matching and Spectral Domain Analysis (SDA). Each technique accounts for a different representation of the electromagnetic field: a discrete sum of modes (series representation for mode-matching) and a continuous sum (integral representation for SDA) [4], [5]. From a practical point of view, the main differences between these two techniques lie in their computational performance (although in practice the use of suitable computational strategies may affect this performance significantly). A crucial point in the two approaches concerns the choice of the waveguide modes in which the electromagnetic fields are expanded (in the SDA, this also determines the inversion contour of the Fourier transform). Different criteria to elucidate this choice have been proposed in the literature, see for example [1], [2], [6]. Nevertheless, to our knowledge, extensive discussion on this fundamental topic has not been reported in the literature. In this paper, we again raise this issue following the discussion presented by the authors in [3]. The problem will be initially posed in the spatial domain, instead of being posed in the spectral domain, in order to consider the current density on the strips as source of the electromagnetic field rather than a boundary condition (such as considered in the conventional SDA). This approach makes possible a fruitful application of *power causality requirements*, which would provide the most realistic description of the behavior of the electromagnetic field in systems with translation symmetry. Thus a basic assumption is that the line field should be built only with those waveguide modes carrying power outward from the source. This requirement besides the consideration of the *nonuniform* nature of the waveguide modes will constitute the core of the present approach.

Once the above choice is made, we apply the Method of Moments in the spectral domain to study the lines. The problem is posed in the spectral domain because of its well-established ability to deal with general multilayered media as well as multiconductor/multislot configurations. The treatment of the leaky regime by means of the above method gives rise to meaningful changes with respect to the treatment of the conventional guided regime. The most significant changes are also discussed in some extent. Specifically, the application of the Parseval's theorem in the SDA is reviewed to take into account the complex nature of the spectral variable and some attention is later devoted to the search for the complex roots of the resulting determinantal equation. These complex zeros account for the complex propagation constants of the line and are found to be located at different sheets of a multivalued function. This fact complicates the zero-searching process and makes necessary the use of more efficient strategies. Finally, comparison with previously published results is presented and some results are reported for the propagation characteristics of a pair of coupled strips both in coplanar and noncoplanar configurations.

Manuscript received April 7, 1994; revised July 25, 1994. This work was supported by DGICYT, Spain, Project TIC91-1018.

The authors are with the Grupo de Microondas, Departamento de Electrónica y Electromagnetismo, Facultad de Física, Universidad de Sevilla, 41012 Sevilla, Spain.

IEEE Log Number 9408565.

II. Analysis

Let us review in this section the basic steps involved in the SDA of the bound and leaky propagation regimes of a

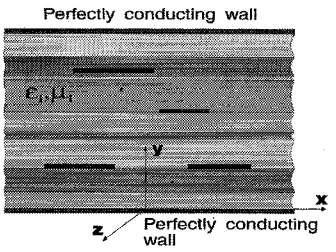

Fig. 1. Cross-section of a planar multiconductor transmission system embedded in a lossless layered medium with top and bottom perfectly conducting walls.

planar transmission system like that shown in Fig. 1. This transmission system is composed of noncoplanar conducting strips embedded in a layered *lossless* medium bounded by top and bottom perfectly conducting plates. The present work will be basically focused on the study of lateral radiation and in this way, the presence of these conducting plates is especially suitable since they prevent spatial radiation and make the mathematical treatment easier. It should be noted that if the usual *time-harmonic regime* is assumed, the treatment of the covered and the uncovered cases conceptually differs because the uncovered case is not merely the limiting case of the covered one when the top conducting plate is removed to infinity. This implies that the lateral radiation of the covered and uncovered cases may be significantly different. Thus a deeper insight into the lateral radiation mechanism could be achieved if the covered case is directly studied instead of analyzing that part of the total radiation corresponding to the surface waves present in the uncovered case.

First, we discuss the integral representation of the spatial Green's function of the structure of Fig. 1 without conductor strips; the remaining layered waveguide will be called the *background* waveguide. This integral representation will determine the proper inversion contour to define the inverse Fourier transform. Later, some relevant aspects related to the application of the Method of Moments and the search for complex roots are considered.

A. Integral Representation of Green's Function

Consider the transmission system of Fig. 1. The substrate of this structure is assumed to be *lossless* and isotropic/anisotropic but with *rotational symmetry* around they y-axis (or in the (x,z)-plane, which will be denoted as the *transverse* plane and represented by the subscript T). As is well known, the transverse (to y) electric and magnetic fields $\boldsymbol{E}_T, \boldsymbol{H}_T$ of the above structure can be derived from certain scalar-mode functions if the layered medium is made of isotropic or anisotropic (satisfying the aforementioned symmetry condition) layers [4], [5], [7]. The introduction of these scalar-mode functions permits the definition of LSE and LSM modes. Thus we first deal only with scalar-mode functions.

Our first purpose will be the computation of the dyadic Green's function, $\bar{\boldsymbol{G}}(x,y;x',y')$, which relates the transverse (to y) part of the electric field to surface current, $\boldsymbol{J}_T(x,y)$, contained in some transverse $y = y'$ plane of the structure in Fig. 1

$$\boldsymbol{E}_T(x,y) = \int \bar{\boldsymbol{G}}(x,y;x',y') \cdot \boldsymbol{J}_T(x',y')\, dx'. \tag{1}$$

We will assume a source and field dependence for the z and t variables of the type $e^{j(\omega t - k_z z)}$, where $k_z = \beta_z + j\alpha_z$ represents the complex propagation constant along the z-direction and ω the angular frequency. The usual case of losses along the z-axis is accounted for by assuming $\beta_z > 0$ and $\alpha_z < 0$.

As mentioned above, any field in the waveguide can be derived from y-directed LSE and LSM modes. This means that the dyadic Green's function can also be derived from certain scalar-mode Green's functions. The derivation of these scalar Green's functions are readily accomplished if the *sources* and *fields* of our problem are redefined. The new *sources* are denoted as F_ϵ and F_μ, and the new *fields* as W_ϵ and W_μ, in such a way that

$$F_\epsilon = \nabla_T \cdot \boldsymbol{J}_T = -j\omega\rho \tag{2}$$

$$F_\mu = (\nabla_T \times \boldsymbol{J}_T) \cdot \boldsymbol{a}_y \tag{3}$$

$$W_\epsilon = \nabla_T \cdot \boldsymbol{E}_T = -\frac{\partial E_y}{\partial y} \tag{4}$$

$$W_\mu = \nabla_T \times \boldsymbol{E}_T = -j\omega\mu H_y \tag{5}$$

where

$$\nabla_T = \boldsymbol{a}_x \frac{\partial}{\partial x} + \boldsymbol{a}_z \frac{\partial}{\partial z}.$$

This transformation is essentially the same as that proposed in [8] (TTL method) when the problem is posed in the spectral domain.

The new W_ϵ and W_μ *fields* satisfy the boundary conditions imposed on the LSM and LSE modes separately. Thus the use of the transformation (2)–(5) diagonalizes the dyadic Green's function

$$W_{\epsilon,\mu}(x,y) = \int g_{\epsilon,\mu}(x,y;x',y') F_{\epsilon,\mu}(x',y')\, dx' \tag{6}$$

where $g_{\epsilon,\mu}(x,y;x',y')$ are the new scalar Green's functions and subscripts ϵ and μ will refer to LSM and LSE modes, respectively. If the involved layered medium has rotational symmetry around the y-axis, this diagonalization works properly when the layers are isotropic and/or uniaxial anisotropic [9]. If gyrotropic layers are present, the transformation (2)–(5) yields nondiagonal expressions for the Green's dyad and consequently scalar Green's functions cannot be defined in this case. Nevertheless, a similar analysis could still be accomplished if the vectorial nature of sources and fields (as well as the dyadic nature of the Green's function) is taken into account.

The scalar-mode Green's function $g_{\epsilon,\mu}(x,y;x',y')$ (generically denoted as g) is found to be the solution of the following scalar-wave equation:

$$\left[\frac{\partial^2}{\partial x^2} + \frac{\partial^2}{\partial y^2} + (\kappa^2 - k_z^2)\right] g(x,y;x',y') = \delta(x-x')\delta(y-y') \tag{7}$$

($\kappa^2 = \omega^2\epsilon\mu$) when subjected to the appropriate boundary conditions.

The two-dimensional scalar-mode Green's function $g(x, y; x', y')$ can be represented via two associated characteristic one-dimensional Green's functions $g_x(x, x')$ and $g_y(y, y')$ [4], [5] as

$$g(x,y;x',y') = \frac{-1}{2\pi j}\oint_{C_x} g_x(x,x';\lambda_x)g_y(y,y';\Gamma^2-\lambda_x)\,d\lambda_x = \frac{-1}{2\pi j}\oint_{C_y} g_x(x,x';\Gamma^2-\lambda_y)g_y(y,y';\lambda_y)\,d\lambda_y$$

where $\lambda_x+\lambda_y = \kappa^2-k_z^2 = \Gamma^2$ and C_x is an integration contour in the complex λ_x plane that encloses, in the positive sense, all the singularities of g_x and excludes all the singularities of g_y; similarly, C_y encloses only the singularities of g_y.

Owing to the cumbersome calculations involved in the treatment of the general structure of Fig. 1, we will first analyze a simpler isotropic and homogeneous parallel-plate waveguide. The analysis of this structure will clarify the main steps of our approach since the procedure is basically the same as that necessary for the general case.

If, for example, we are interested in the LSM-mode scalar Green's function, g_ϵ can be expressed as [4]

$$g_\epsilon(x,y;x',y') = \frac{1}{2\pi j}\oint_{C_x}\frac{je^{-j\sqrt{\lambda_x}|x-x'|}}{b\sqrt{\lambda_x}} \times \sum_{m=1}^{\infty}\frac{\sin\left(\frac{m\pi}{b}y\right)\sin\left(\frac{m\pi}{b}y'\right)}{\lambda_x-\left[\Gamma^2-\left(\frac{m\pi}{b}\right)^2\right]}\,d\lambda_x. \quad (8)$$

The integrand in (8) is a two-valued complex function in the λ_x-plane with a branch point at $\lambda_x = 0$ and poles located at $\lambda_{x,m} = \Gamma^2-(m\pi/b)^2$ on both sheets of the Riemann surface. The $\lambda_{x,m}$ poles can be rewritten as

$$\lambda_{x,m} = \gamma_{g,m}^2 - k_z^2 \quad (9)$$

where $\gamma_{g,m}^2 = \kappa^2-(m\pi/b)^2$ is the squared transverse wavenumber of the mth source-free LSM-mode of the homogeneous parallel-plate waveguide. Note that $\gamma_{g,m}$ would directly account for the phase constant if the corresponding mode is uniform. On the contrary, as will become apparent later, this variable should not be identified as the phase constant of a nonuniform mode [10] (we denote a nonuniform waveguide mode as that propagating in a given direction and attenuating/growing in the perpendicular one).

As noted in [5, p. 278], the two-valued function, $g_x(x, x', \lambda_x)$, must be defined in such a way that it decays to zero when $|\lambda_x|$ goes to infinity on the top sheet. This requirement is fulfilled when the branch cut tends for large values of Re (λ_x) to the positive real axis but an infinitesimal distance above it. A usual choice of this branch cut defines the top sheet of the Riemann surface defined by $\sqrt{\lambda_x}$ function in (8) as that where

$$\text{Im}\sqrt{\lambda_x} < 0. \quad (10)$$

This sheet is usually known as *spectral* sheet. Since the integration path in (8) must enclose only the singularities of g_x, C_x must then enclose the branch cut in the positive sense and exclude all the poles of g_y, as shown in Fig. 2. The above choice of the branch cut is simply one possible definition. From our standpoint, the most convenient choice should be decided on physical grounds.

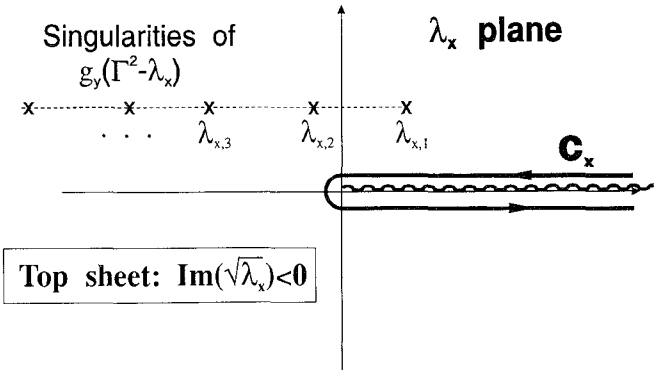

Fig. 2. Integration path, C_x, on the spectral sheet of the λ_x-plane.

Note that for $x \neq x'$ (i.e., outside the line source), the integral (8) over the radius infinity is zero provided the condition reported in [5, p. 278] is fulfilled. Therefore, the integral contour can be alternatively closed following the circle $|\lambda_x| \to \infty$ on the *spectral* sheet. The integral representation of $g_x(x, x', \lambda_x)$ is thus transformed into a sum of residues at the poles on the *spectral* sheet, that is

$$g_\epsilon(x,y;x',y') = \frac{j}{b}\sum_{m=1}^{\infty}\frac{\sin\left(\frac{m\pi}{b}y\right)\sin\left(\frac{m\pi}{b}y'\right)}{k_{x,m}}e^{-jk_{x,m}|x-x'|} \quad (11)$$

where

$$k_{x,m} = \beta_{x,m} + j\alpha_{x,m} = \sqrt{\gamma_{g,m}^2 - k_z^2}. \quad (12)$$

This leads to a mode expansion of the scalar Green's function whose modes are considered with

$$\text{Im}\sqrt{\gamma_{g,m}^2 - k_z^2} < 0.$$

The fields due to a line source at $x = x'$ are then written as a superposition of evanescent (in the x-direction) modes of the *background* waveguide. Since all these modes also propagate along the z-direction with a propagation constant k_z, they are actually *nonuniform* modes.

The above expansion of the fields is found appropriate for the analysis of the purely propagating modes (namely, the bound modes) of the transmission system of Fig. 1. Nevertheless, if we are interested in the analysis of the leaky regime, the above expansion does not properly describe the growing field behavior for $|x| \to \infty$. Therefore, a different integral representation (i.e., a different branch cut choice) should be considered. As was noted above, any other integration contour enclosing a different branch cut but having the same initial and final points (i.e., $g_x(x, x', \lambda_x) \to 0$ when $|\lambda_x| \to \infty$) would provide a mathematically consistent integral representation of the Green's function, and this different integral representation would also lead to a different modal expansion. We are only interested in that mathematical solution compatible with the fact that point (x', y') be a source rather than a sink. In other words, if the propagation constant of the line along z is real

($\alpha_z = 0$), the above condition is fulfilled if $\mathrm{Im}\,(k_{x,m}) < 0$ and therefore all the modes behave like evanescent waves along the x-direction. If k_z is assumed to be complex, the propagation constant of each mode along the x-direction, $k_{x,m}$, is also complex ($k_{x,m} = \beta_{x,m} + j\alpha_{x,m}$) and consequently energy is transferred in the x-direction by *all* waveguide modes. In this case, point (x', y') constitutes a source provided that the modal expansion (11) is formed exclusively by modes carrying power outward from this point. The criterion to decide which modes should be included in (11) must then be related to the direction of the power flux associated with each nonuniform mode. This criterion will be named the *criterion of outgoing power*. Since the same question arises concerning the proper expansion of the field in terms of waveguide modes and the proper choice of the branch cut, we first consider the discrete mode expansion of the scalar Green's function—see (11)—to decide later the integration contour on physical grounds.

Taking for simplicity $x' = 0, y' = 0$, the scalar-mode Green's function, $g_\epsilon(\boldsymbol{r}) = g_\epsilon(x, y)\exp(-jk_z z)$, can be written as the following expansion in terms of nonuniform and orthogonal LSM-modes:

$$g_\epsilon(\boldsymbol{r}) = \sum_{m=1}^{\infty} a_m(y) e^{-j(k_{x,m}\boldsymbol{a}_x + k_z \boldsymbol{a}_z)\cdot\boldsymbol{\rho}} \tag{13}$$

where $\rho = |x|\boldsymbol{a}_x + z\boldsymbol{a}_z$. If the complex wavevector $\boldsymbol{k}_m = k_{x,m}\boldsymbol{a}_x + k_z\boldsymbol{a}_z$ is defined, the above expression is rewritten as

$$g_\epsilon(\boldsymbol{r}) = \sum_{m=1}^{\infty} a_m(y) e^{-j\boldsymbol{k}_m\cdot\boldsymbol{\rho}} \tag{14}$$

with $\boldsymbol{k}_m$ satisfying the equation

$$k_{x,m}^2 + k_z^2 = \boldsymbol{k}_m \cdot \boldsymbol{k}_m = \gamma_{g,m}^2. \tag{15}$$

The $\boldsymbol{k}_m$ complex vector can also be written as a sum of a real and a complex vector

$$\boldsymbol{k}_m = \beta_m \boldsymbol{u}_m + j\alpha_m \boldsymbol{v}_m \tag{16}$$

where $\beta_m\boldsymbol{u}_m = \beta_{x,m}\boldsymbol{a}_x + \beta_z\boldsymbol{a}_z$ and $\alpha_m\boldsymbol{v}_m = \alpha_{x,m}\boldsymbol{a}_x + \alpha_z\boldsymbol{a}_z$ are *real* vectors whose unitary vectors $\boldsymbol{u}_m$ and $\boldsymbol{v}_m$ define the directions of phase propagation and amplitude attenuation, respectively. From (15) and (16), the above quantities are related by

$$\beta_{x,m}^2 - \alpha_{x,m}^2 = \gamma_{g,m}^2 - (\beta_z^2 - \alpha_z^2) \tag{17}$$

$$\beta_{x,m}\alpha_{x,m} = -\beta_z\alpha_z \tag{18}$$

$$\beta_m^2 = \beta_{m,x}^2 + \beta_z^2 \tag{19}$$

$$\alpha_m^2 = \alpha_{m,x}^2 + \alpha_z^2, \tag{20}$$

which implies that $\boldsymbol{u}_m \cdot \boldsymbol{v}_m = 0$. This latter relation is typical for nonuniform plane waves in lossless media (see, for example, [10, pp. 320–334]) and it establishes the orthogonality between the propagation and attenuation directions.

The expansion given in (14) can also be viewed as the following superposition of infinite nonuniform modes:

$$g_\epsilon(\boldsymbol{r}) = \sum_{m=1}^{\infty} a_m(y) e^{\alpha_{x,m}|x| + \alpha_z z} e^{-j(\beta_{x,m}|x| + \beta_z z)} \tag{21}$$

where the presence of the *modulus* $|x|$ in (21) accounts for the symmetry of the expansion at both sides of the source ($x' = 0$). Note that all the nonuniform modes in (21) are *slower* than the leaky line mode; namely, its phase constants β_m are always greater than the leaky mode phase constant β_z—see (19). Therefore, all the waveguide modes in (21) satisfy the phase match condition.

The above superposition of nonuniform modes fulfills the criterion of outgoing power provided that *all the modes* in the expansion carry power *outward* from the source. This condition will be satisfied when the x-projection of the real part of the Poynting vector associated with each mode $S_{x,m}$ is positive. It can be readily shown (see the Appendix) that

$$P_{x,m} = \mathrm{Re}\,(S_{x,m}) = C^+ \gamma_{g,m}^2 \beta_{x,m} \tag{22}$$

where C^+ is a positive quantity. In view of (18) and providing that $\mathrm{sign}\,(\beta_{x,m}) = \mathrm{sign}\,(\alpha_{x,m})$ (since $\mathrm{sign}\,(\beta_z) = -\mathrm{sign}\,(\alpha_z)$ by hypothesis), the criterion followed to include a mode in expansion (11) can be expressed as

$$\mathrm{sign}\,(\gamma_{g,m}^2 \alpha_{x,m}) = +. \tag{23}$$

Since $\gamma_{g,m}^2$ is a real number in lossless waveguides, the above criterion implies that those modes associated with $\gamma_{g,m}^2 > 0$ should be considered with $\mathrm{Im}\,(k_{x,m}) > 0$; and similarly those corresponding to $\gamma_{g,m}^2 < 0$ with $\mathrm{Im}\,(k_{x,m}) < 0$.

Once the modal expansion has been analyzed, the integration contour of the integral representation (8) should be defined so that both representations are equivalent. This can be achieved if the branch cut is defined in such a way that all the poles associated with the modes in the residue expansion are located on the top sheet. Then, applying the Cauchy integral theorem, the correct modal expansion is recovered. This top sheet will be called *causal sheet* and verifies that

$$\gamma_{g,m}^2\,\mathrm{Im}\,(\sqrt{\lambda_{x,m}}) > 0 \tag{24}$$

for all values of m.

For example, consider the disposition of the $\lambda_{x,m}$ poles shown in Fig. 3, where $\gamma_{g,1}^2 > \mathrm{Re}\,(k_z^2) > \gamma_{g,2}^2 > \gamma_{g,3}^2 > \cdots$ (k_z complex). Assuming that only the first two poles verify that $\gamma_{g,m}^2 > 0$ ($m = 1, 2$), an integration path, C_x, that would yield a *causal* integral representation of the scalar mode Green's function is illustrated in Fig. 3. Another (but equivalent) causal integral representation can be obtained by following a different approach. This approach consists on starting from the definition of the *spectral* sheet (see its definition in (10)) and then to deform the integration path according to the criterion of the outgoing power. In this case, only the $\lambda_{x,m}$ poles associated with $\gamma_{g,m}^2 < 0$ should be considered in the spectral sheet and those associated with $\gamma_{g,m}^2 > 0$ in the bottom sheet (and consequently, they should be then excluded in the top sheet). The integration contour and the above described branch cut are shown in Fig. 4.

If the transformation $k_x^2 = \lambda_x$ is applied to (8) (in reference to any of the integral representations shown in Figs. 3 and 4), g_ϵ turns into the following inverse Fourier transform:

$$g_\epsilon(x, y; x', y') = \frac{1}{2\pi}\int_{C(\omega)} \tilde{g}_\epsilon(k_x, y, y'; k_z) e^{-jk_x(x-x')}\, dk_x \tag{25}$$

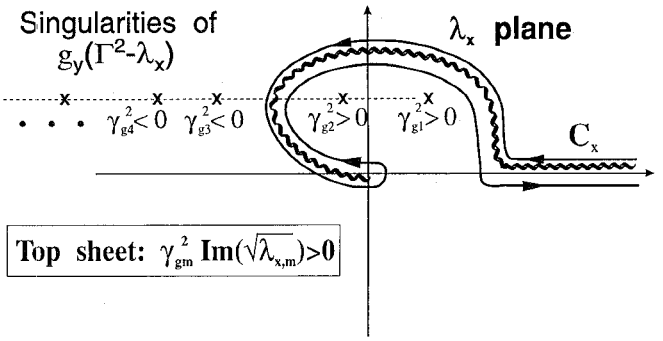

Fig. 3. Integration path C_x on the causal sheet of the λ_x-plane.

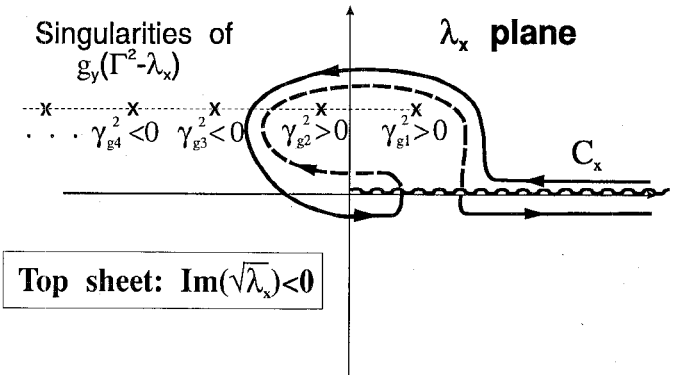

Fig. 4. Integration path C_x equivalent to that of Fig. 3 when the top sheet is defined as the spectral sheet. (- - - - -): path in the botton sheet; (———): path in the top sheet.

where

$$\tilde{g}_\epsilon(k_x,y,y';k_z)=\frac{j}{b}\sum_{m=1}^{\infty}\frac{\sin\left(\frac{m\pi}{b}y\right)\sin\left(\frac{m\pi}{b}y'\right)}{k_x^2-(\gamma_{g,m}^2-k_z^2)} \tag{26}$$

can be considered the *spectral* scalar-mode Green's function with the corresponding inverse integration contour $C(\omega)$ shown in Fig. 5 (an analogous procedure for the LSE-modes would lead to a similar expression for g_μ). It should be noted that the inverse integration contour is only a function of the operating frequency; namely, $C(\omega)$ should properly surround all the poles corresponding to positive squared transverse wavenumbers of the background waveguide. Those poles are located in the shadowed region of Fig. 5 and this region is only determined by the $\beta_{x,m}^2-\alpha_{x,m}^2=\beta_z^2-\alpha_z^2$ hyperbolas. Consequently, $C(\omega)$ does not depend on the height and/or material characteristics of the layer. These parameters only affect the total number of poles surrounded by the previously determined integration contour.

The basic steps of the proceeding development also applies if the general structure of Fig. 1 had been considered. The only changes would appear in a more cumbersome algebraical expression of $g_y(y,y';\lambda_y)$ owing to the boundary conditions at the different interfaces to be now satisfied by $g_\epsilon(y,y';\lambda_y)$. Provided that the scalar LSM- and LSE-mode decomposition holds, the functions $\tilde{g}_{\epsilon,\mu}$ [5], [7] can be still expressed in a closed form similar to (26)

$$\tilde{g}_{\epsilon,\mu}(k_x,y,y';k_z)=\frac{j}{b}\sum_{m=1}^{\infty}\frac{f_m^{\epsilon,\mu}(y)f_m^{\epsilon,\mu}(y')}{k_x^2-(\gamma_{g,m}^2-k_z^2)} \tag{27}$$

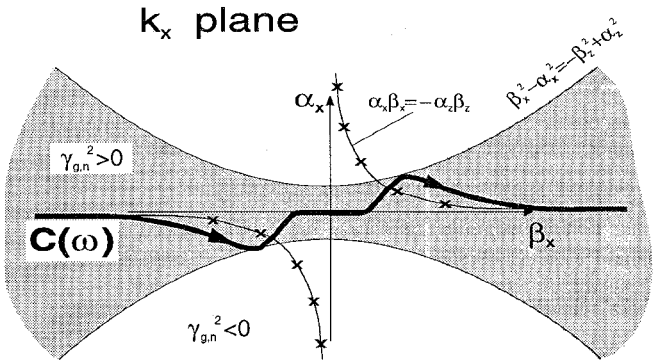

Fig. 5. Integration contour C in the k_x-plane.

where $\gamma_{g,m}^2$ now accounts for the squared transverse wavenumbers of the LSE- and LSM-modes of the general background waveguide and $f_m^{\epsilon,\mu}(y)$ for the corresponding ϵ,μ eigenfunctions along the y-direction.

Once the spectral scalar-mode Green's functions and the proper inversion contour to be used in the Fourier transform have been determined, the spatial dyadic Green's function (1) $\bar{\boldsymbol{G}}(x,y;x',y')$ of the general waveguide is obtained by reversing the transformations (2)–(5). However, this process is more readily accomplished in the spectral domain and thus we first reverse the transformation in the spectral domain. Later, $\bar{\boldsymbol{G}}(x,y;x',y')$ can be recovered by means of its integral representation

$$\bar{\boldsymbol{G}}(x,y;x',y')=\frac{1}{2\pi}\int_{C(\omega)}\tilde{\bar{\boldsymbol{G}}}(k_x,y,y';k_z)e^{-jk_xx}\,dk_x \tag{28}$$

where the spectral dyadic Green's function (SDGF) is given by

$$\tilde{\bar{\boldsymbol{G}}}(k_x,y,y';k_z)=[\boldsymbol{Q}]^{-1}\cdot\begin{bmatrix}\tilde{g}_\epsilon & 0\\ 0 & \tilde{g}_\mu\end{bmatrix}\cdot[\boldsymbol{Q}] \tag{29}$$

with $[\boldsymbol{Q}]$ being the matrix associated with the transformation (2)–(5) in the spectral domain, that is

$$[\boldsymbol{Q}]=\begin{bmatrix}-jk_x & -jk_z\\ -jk_z & jk_x\end{bmatrix} \tag{30}$$

and the inversion contour $C(\omega)$ is that found for the scalar Green's function.

Besides the above formal procedure to obtain $\tilde{\bar{\boldsymbol{G}}}(k_x,k_z)$, there are many examples in the literature concerning the computation of the SDGF of layered planar structures (see [11]–[13] and references therein). In most of these methods, the problem is directly posed in the spectral domain and then the surface current density is considered as a boundary condition rather than a source. These methods are found advantageous since they provide the SDGF for very general structures (even if LSE/LSM-mode decomposition is not possible). However, they do not say anything about the appropriate inversion contour. This is the main reason why the source has been explicitly taken into account in the present analysis.

The spatial transverse (to y) electric field, $\boldsymbol{E}_T(x,y)e^{-jk_zz}$, produced by a certain transverse current distribution, $\boldsymbol{J}_T(x,y)e^{-jk_zz}$, can then be expressed (after applying Parseval's theorem) as

$$\boldsymbol{E}_T(x,y)=\frac{1}{2\pi}\int_{C(\omega)}\tilde{\bar{\boldsymbol{G}}}(k_x,k_z)\cdot\tilde{\boldsymbol{J}}_T(k_x)\,e^{-jk_xx}\,dk_x. \tag{31}$$

In the above expression, $\tilde{\tilde{\boldsymbol{G}}}(k_x, k_z)$ represents the analytical extension of the usual SDGF (which could be readily computed following the EBM technique shown in [13], [14]) and $C(\omega)$ is that integration contour satisfying the criterion of outgoing power discussed above.

B. Method of Moments

As is well known, the application of Galerkin's method to the analysis of the transmission system shown in Fig. 1 leads to a homogeneous matrix eigenvalue problem. The elements of the eigenvectors of this problem are the coefficients of the expanded excitation and the eigenvalues, which are the zeros of a determinantal function, represent the modal propagation constants of the transmission system. Each element of the Galerkin matrix, Γ_{pq}, can be formally expressed as

$$\Gamma_{pq} = \int_{-\infty}^{\infty} \boldsymbol{J}^*_{T,p}(x) \cdot \boldsymbol{E}_{T,q}(x)\, dx \tag{32}$$

where the subscripts p and q refer to the pth and qth strips and the complex conjugation is introduced to be consistent with the inner product definition. If we now express the transverse electric field in terms of the integral representation given by (31) and inverting the integration order, (32) becomes

$$\Gamma_{pq} = \frac{1}{2\pi} \int_C \left[\int_{-\infty}^{\infty} \boldsymbol{J}^*_{T,p}(x)\, e^{-jk_x x}\, dx \right] \cdot \tilde{\tilde{\boldsymbol{G}}}(k_x, k_z) \cdot \tilde{\boldsymbol{J}}_{T,q}(k_x) dk_x. \tag{33}$$

Taking into account the complex nature of the k_x variable and the complex nature of the Fourier transform of the current density $\tilde{\boldsymbol{J}}_T$ (which should be considered a complex function of a complex variable), (33) can be rewritten as

$$\Gamma_{pq} = \frac{1}{2\pi} \int_C \tilde{\boldsymbol{J}}^*_{T,p}(k_x^*) \cdot \tilde{\tilde{\boldsymbol{G}}}(k_x, k_z) \cdot \tilde{\boldsymbol{J}}_{T,q}(k_x)\, dk_x. \tag{34}$$

Note that all the singularities of the integrand of (34) stem from the poles of SDGF since $\tilde{\boldsymbol{J}}_{T,\nu}(k_x)$ is a uniform and analytic function. It is also relevant to emphasize that the presence of the double complex-conjugation in (34), and similarly in all the problems treated in the SDA when the spectral variable is assumed complex, has two significant effects:

1) It preserves the symmetry properties of the coefficients of Galerkin matrix; namely, it is assured that $\Gamma_{pq} = \Gamma^*_{qp}$ if k_z is real and $\Gamma_{pq} = \Gamma_{qp}$ if k_z is complex.
2) It makes the integrand in (34) satisfy the Cauchy–Riemann conditions (except at the singularities of the SDGF) with the integrand being a meromorphic complex function. This requirement will assure that $C(\omega)$ can be freely deformed if no poles are crossed. Assuming that $\tilde{\boldsymbol{J}}_{T,\nu}(k_x)$ is analytic, the proof of the meromorphic nature of the integrand in (34) reduces then to show that $\tilde{\boldsymbol{J}}^*_{T,\nu}(k_x^*)$ is also analytic. If any of the components of $\tilde{\boldsymbol{J}}_{T,\nu}(k_x)$ is denoted as $f(z)$, according to the complex variable theory this function can be expressed in terms of a convergent series of z, namely

$$f(z) = \sum A_n z^n.$$

Note that the function

$$g(z) = f^*(z) = \sum A_n^* (z^*)^n$$

is not analytic since it is not possible to express $g(z)$ in terms of a series of z. However, the function

$$h(z) = f^*(z^*) = \sum A_n^* z^n$$

can again be expressed as another convergent series of z (with the same convergence radius than $f(z)$) and therefore $f^*(z^*)$ is found to be analytic.

Once we have found the proper integrand and integration contour of (34), this integral should be efficiently computed. One of the most extended ways of treating (34) consists on deforming the original integration contour into the real axis and later to add the residues of the involved poles [15]. Nevertheless, this technique yields *overflow* computational problems when the poles are located nearby the real axis (as it often occurs). In our experience and similar to [16], this drawback is readily overcome if we first subtract out the contribution of the poles and this contribution is later added. The application of this scheme makes the numerical computation quite easy owing to the smooth behavior of the remaining integrand. The use of some additional asymptotic techniques is usually unavoidable to achieve accuracy and reduced CPU times [14].

C. Root Searching in the Complex k_z-Plane

Once all the elements of the Galerkin's matrix have been computed, the propagation constants of the transmission system are obtained (for a fixed value of ω) as the complex zeros of

$$\Psi(k_z) = \det\left[\Gamma_{pq}(k_z; \omega)\right] = 0. \tag{35}$$

It is important to note, upon observing (29) and (34), that $\Psi(k_z)$ can be expressed in terms of the following series:

$$\Psi(k_z) = \sum_{m=1}^{\infty} \Psi_m(k_z) = \sum_{m=1}^{\infty} \int_C \frac{Q_m(k_x)}{k_x^2 - (\gamma_{g,m}^2 - k_z^2)}\, dk_x \tag{36}$$

where each $Q_m(k_x)$ is an analytic function (no poles or branch points). Each term of (36) shows the generic form

$$\Psi_m(k_z) = \int_C \frac{Q_m(k_x)}{k_x^2 - \xi_m^2}\, dk_x \tag{37}$$

where $\xi_m^2 = \gamma_{g,m}^2 - k_z^2$. This latter integral defines a two-valued function in the k_z complex plane with a branch point at $k_z^2 = \gamma_m^2$ (namely, when $\xi_m = 0$). If the integration path C is defined in such a way that the pole of the integrand denoted as ξ_m^+ is below C and ξ_m^- above C, the multivalued nature of (37) can be understood by observing that the two situations illustrated in Fig. 6 correspond to two different and indistinguishable pole locations. The function defined in (37) shows two values (associated with the two different integration contours) for the same value of k_z.

Note that the definition of the branch cut of the Riemann surface in the k_z-plane is closely related to the choice of the integration contour in the k_x-plane. The top sheet of

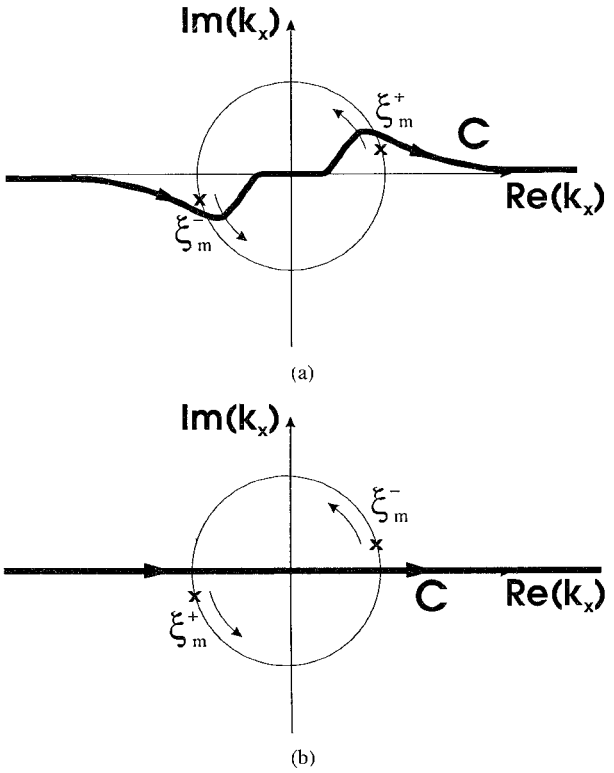

Fig. 6 Two possible integration paths corresponding to identical pole locations.

the k_z-plane (also called a *proper* sheet) is associated with an integration along the entire real axis (see Fig. 6(b)) and the second sheet (an *improper* sheet) with an integration partially along the real axis (see Fig. 6(a)). Assuming the two-valued nature of each $\Psi_m(k_z)$ term, the $\Psi(k_z)$ function will have infinite branch points in the k_z-plane at $k_z = \pm\gamma_{g,m}$ $(m = 1, 2, \cdots)$. Since there are a finite number of positive values of $\gamma_{g,m}^2$ and an infinite number of negative ones [4], [7], the $\Psi(k_z)$ function will have several branch points at the real axis and infinite branch points at the imaginary axis.

Owing to the multivalued nature of $\Psi(k_z)$ function, the zero-searching process becomes much more involved than in the single-valued case. Thus it will be necessary to analyze the different sheets of the Riemann surface since the roots can be located on any of them. Note that the study of the different sheets in the k_z-plane is related to the computation of (36) with different choices of the integration contour. Nevertheless, and in spite of the different mathematical solutions satisfying $\Psi(k_z) = 0$ (often one on each sheet for each mode), only those solutions located on the *causal* sheets of the k_z-plane should be considered. The *causal* sheet in this k_z-plane comes determined by an appropriate choice of the integration contour of (36) in the k_x-plane; this contour should be chosen according to the modal causality requirements discussed above for the integral representation of the Green's function. The proposed criterion would imply that if k_z is real ($\alpha_z = 0$) the integration path should be taken along the entire real axis and then the causal sheet would be the top sheet. On the other hand, if k_z is complex, all those poles associated with waveguide modes verifying $\gamma_{g,m}^2 > 0$ should be properly surrounded by the integration contour (as in the case depicted in Fig. 5). This requirement would lead directly to the causal sheet (in the k_z-plane) where the root searching should be carried out. Nevertheless, in our propagation problem we do not know the actual location of the propagation constant k_z until the zero-searching process has finished; and therefore, we would have to look for zeros in different noncausal sheets.

The usual methods of searching for complex zeros of a complex function (integral methods based on Cauchy theorem [17], differential methods such as Muller's method, or those based on single-valued decomposition [18]) work properly only in regions where the function is analytic. Consequently, it would be very desirable to apply some transformation to turn the multivalued $\Psi(k_z)$ function into a single-valued function. Unfortunately, this transformation (also the mapping of this transformation) is very involved since $\Psi(k_z)$ has infinite branch points. However, from a practical viewpoint, we can distinguish two cases in function of the number of waveguide modes verifying $\gamma_{g,m}^2 > 0$ at a given frequency.

1) *Only One Waveguide Mode Verifying* $\gamma_{g.m}^2 > 0$: If only one squared transverse wavenumber is positive (at least one always satisfies this condition), the causal sheet can be one of the two sheets (or the two of them) related to the first branch point $k_z = \pm\gamma_{g,1}$. In this case, it is useful to introduce a new complex variable ϕ via the transformation

$$k_z = \gamma_{g,1} \sin\phi. \tag{38}$$

A discussion of this transformation can be found in [5]. When (38) is applied to (36), the branch point $k_z = \pm\gamma_{g,1}$ turns into a pole at $\pm\pi/2$ and the two possible causal sheets of the k_z-plane appear as adjacent and periodic regions in the top sheet of the new ϕ-plane. The root searching can be then restricted to the region bounded by $0 < \mathrm{Re}\,(\phi) < 2\pi$. Moreover, any root searching method would work efficiently in this region of the ϕ-plane (eliminating previously the pole at $\pm\pi/2$), which now accounts for the proper and first improper sheets of the k_z plane.

2) *More Than One Waveguide Mode Verifying* $\gamma_{g,m}^2 > 0$: Assuming that ν waveguide modes verify $\gamma_{g,m}^2 > 0$ $(m = 1, \cdots, \nu)$, the causal sheets can be both the top sheet and the 2νth sheet. These two sheets are associated, respectively, with an integration contour in the k_x-plane along the real axis (see Fig. 7(a)) and with an integration contour surrounding the ν poles corresponding to positive values of $\gamma_{g,m}^2 > 0$ (see Fig. 7(b)). This means that if the final value of k_z is real (and consequently $k_z^2 > \gamma_{g,1}^2$), the causal sheet is the top one and if k_z is complex, the causal sheet is therefore the 2νth sheet. To our knowledge, there is no easy transformation that can map the two causal sheets of the k_z-plane into adjacent regions in a new complex plane. Therefore, the zero-searching process should be made directly on the first sheet or on the 2νth sheet of the k_z-plane.

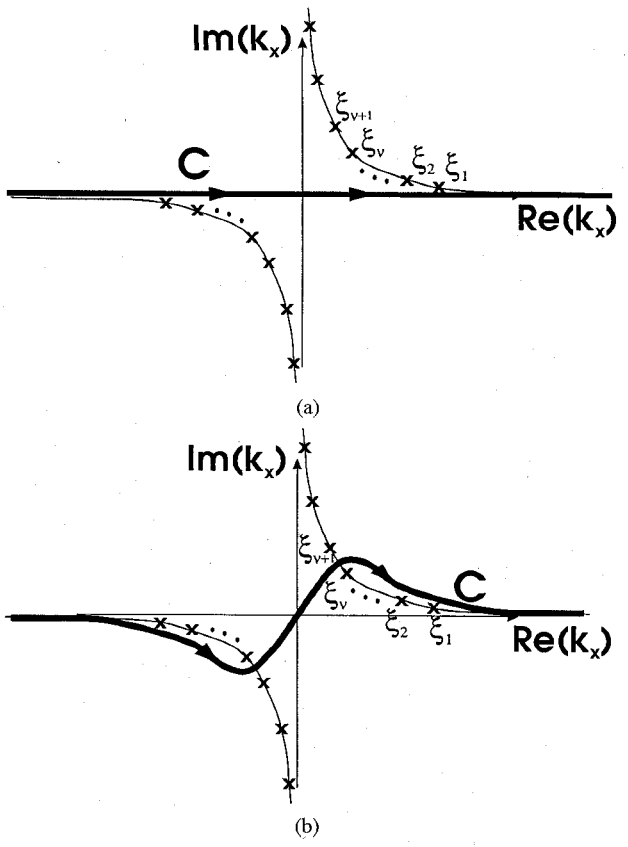

Fig. 7. Integration contours corresponding to the two possibilities of causal integral representations when there are ν positive squared waveguide wavenumbers.

III. Numerical Results

In this section, we present some numerical results obtained by a computer code implementing the theory of the preceeding section. The results so obtained may differ from the previously published data since other authors could have used different criteria in the definition of the inversion contour of the Fourier transform and in the application of the Parseval's theorem. First for comparison, we analyze the inhomogeneous stripline previously treated in [19]. This work studied and confirmed experimentally the existence of a leaky dominant mode in a stripline with a small airgap above the strip. Fig. 8 shows our results for the normalized (to $k_0 = w\sqrt{\epsilon_0\mu_0}$) propagation constants of the dominant leaky mode together with those extracted from [19, Fig. 2]. A good agreement is found for the two sets of numerical results in the whole analyzed range. This numerical agreement is expected because the present structure has only one waveguide mode with $\gamma_g^2 > 0$. In this case, most of the published works (including the present paper) follow the same criterion for the definition of the inversion contour. On the contrary, as was noted above, numerical and qualitative discrepancies could appear when more than one waveguide mode satisfies $\gamma_g^2 > 0$. A relevant feature of the results in Fig. 8 is the presence of values of the leaky mode phase constant β_z greater than the wavenumber of the fundamental waveguide mode. This unconventional leakage can be explained if the nonuniform nature of the modes in (21) is considered. From (21) and (17)–(20), the phase constant of the dominant waveguide mode excited by the leaky line mode

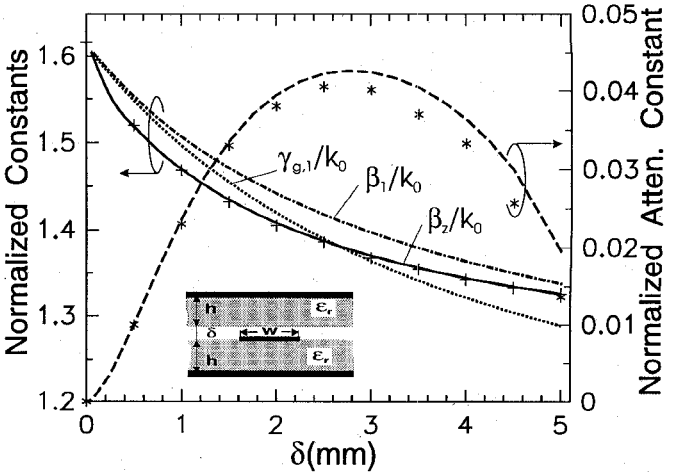

Fig. 8. Normalized phase constant (solid line) and attenuation constant (dashed line) of the leaky mode for an inhomogeneous stripline at 3 GHz versus the height of the airgap ($h = 4.45$ mm; $w = 6.35$ mm). Solid and dashed lines: our results; asterisks and crosses: results of [19]; dotted line: normalized wavenumber; and dotted–dashed line: normalized phase constant of the dominant nonuniform parallel-plate mode.

is β_1 (given by (19) with $m = 1$) rather than $\gamma_{g,1}$. The values of β_1, obtained from (17)–(20), are also shown in Fig. 8. It can be seen how the leaky line mode is always faster than the dominant nonuniform background waveguide mode.

An example of the differences that can be found when different inversion contours are used is shown in Fig. 9. This figure shows the differences found in the propagation constant characteristics of the leaky mode of a pair of coupled strips. The (a) family of curves accounts for the real and imaginary parts of the complex propagation constant of the leaky mode when the inversion contour is chosen as that surrounding only the pole associated with the dominant parallel-plate mode. These curves could not have physical meaning according to the viewpoint proposed here since they have been computed by violating the criterion of the outgoing power. On the other hand, the (b) family of curves accounts for the behavior of the complex propagation constant of the leaky mode when the inversion contour surrounds all the poles associated with positive values of the squared transverse wavenumber of the parallel-plate waveguide. Although the phase constants β_m of the different waveguide modes corresponding to $\gamma_{g,m}^2 > 0$ have not been plotted, it has been checked that the leaky line mode is always faster than all the excited nonuniform background waveguide modes.

Finally, Fig. 10 illustrates the leakage characteristics of one of the fundamental modes of a pair of *noncoplanar* strips as a function of the center separation. This figure shows both the normalized phase and attenuation constants for three values of frequencies (only one parallel-plate mode is above cutoff for the dimensions and frequencies analyzed). The three different curves corresponding to the behavior of β_z/k_0 for the three values of frequencies appear superimposed, that is, the phase constant of this mode is hardly dispersive. On the contrary, it can be seen how the leakage losses are highly affected by the frequency. This fact may seriously restrict the technological application of this type of noncoplanar configuration in miniaturized microwave devices even for typical transversal dimensions much less than the vacuum wavelength. We have

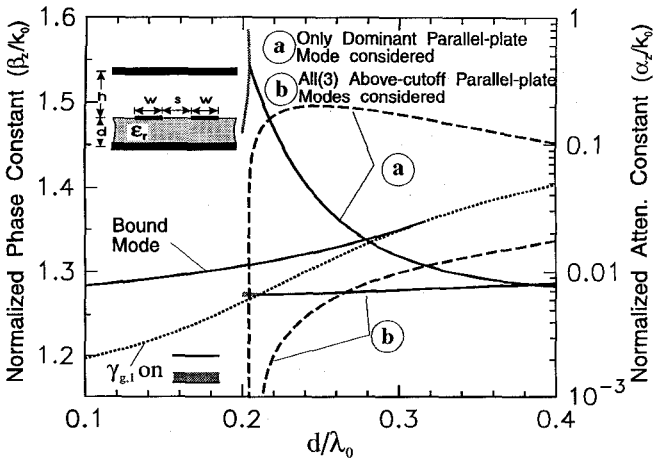

Fig. 9. Normalized phase constant (β_z/k_0: solid lines) and normalized attenuation constant (α_z/k_0: dashed lines) for the odd mode of a pair of coplanar coupled strips where $\epsilon_r = 2.25, w/d = 0.50, s/d = 0.25, h/d = 1$. Dotted line: normalized wavenumber $\gamma_{g,1}$ of the dominant parallel-plate mode. Grey lines: real improper modes.

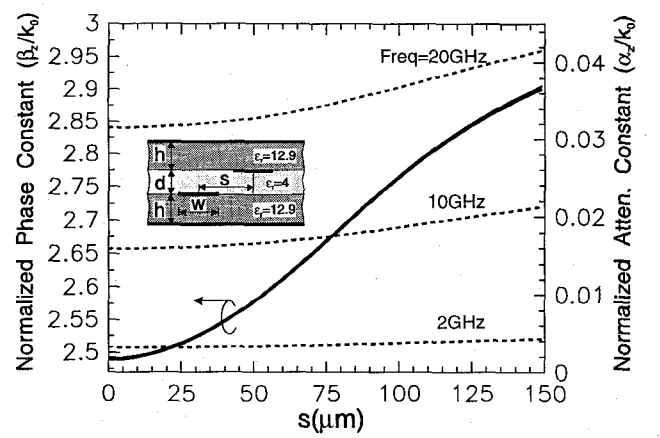

Fig. 10. Normalized phase constant (β_z/k_0: solid lines) and normalized attenuation constant (α_z/k_0: dashed lines) for the lower fundamental mode of a pair of noncoplanar coupled strips where $w = 80\ \mu$m, $h = 200\ \mu$m, $d = 50\ \mu$m.

found (similarly to [2]) that many noncoplanar multiconductor configurations show this trend to leak laterally. Consequently, the numerical study of the propagation characteristics in these laterally open and noncoplanar structures should be carefully made. In particular, the possible leakage effects should be predicted in order to either prevent or take advantage of them.

IV. Conclusion

This work has analyzed the possible definitions of the inversion contour of the Fourier transform when this integral transform is applied to the analysis of the electromagnetic propagation in covered planar transmission systems with translation symmetry. We propose an approach starting from that integral representation of the spatial LSE/LSM scalar-mode Green's function which only comprises waves transferring energy away from the source. This integral representation can be later transformed to be viewed as an inverse Fourier transform. Thus it renders the inversion contour of the Fourier transform in an unambiguous and direct way. For stratified structures, the spectral dyadic Green's function for complex values of the spectral variable can be easily computed as the analytical continuation of those spectral dyadic Green's functions previously reported in the literature for real values of the spectral variable.

Some relevant theoretical and numerical aspects related to the application of the Galerkin method in the spectral domain to the study of the leaky regime have been discussed. Some attention has also been devoted to the zero-searching method since the complex propagation constants of the leaky modes appear on different sheets of a multivalued function.

Finally, some numerical results show a good agreement between our results and previously published data. We have also presented an example to show the quantitative and qualitative differences that can be found for the propagation characteristics when different choice of the inverse Fourier contour are used. In addition, the leaky behavior of noncoplanar covered structures has been analyzed, the high tendency of these structures to leak laterally even for typical dimensions much less than the vacuum wavelength has been found.

Appendix

Let $\boldsymbol{E}, \boldsymbol{H}$ be the fields of a nonuniform mode which verifies certain boundary condition in the y-direction and whose transverse complex propagation constant is given by $\boldsymbol{k}_T = k_x \boldsymbol{a}_x + k_z \boldsymbol{a}_z$. The Poynting vector in the x-direction, $\boldsymbol{S}_x$, is given by

$$S_x = E_y H_z^* - E_z H_y^*. \tag{39}$$

If only LSM-modes are now considered, (39) reduces to $S_x^\epsilon = E_y H_z^*$. From $\nabla \times \boldsymbol{H} = j\omega\epsilon \boldsymbol{E}$ and $\nabla \cdot \boldsymbol{H} = 0$, it follows that

$$E_y = -\frac{k_z}{\omega\epsilon} H_x + \frac{k_x}{\omega\epsilon} H_z \qquad H_x = -\frac{k_z}{k_x} H_z \tag{40}$$

and substituting (40) into (39)

$$S_x^\epsilon = \frac{k_x^*}{\omega\epsilon |k_x|^2} \left(k_x^2 + k_z^2\right) |H_z|^2. \tag{41}$$

Upon considering that the squared transverse wavenumber is $\gamma_g^2 = k_x^2 + k_z^2$ (similar to (12)), the x-component of the Poynting vector associated with LSM-modes can be written as

$$S_x^\epsilon = \frac{1}{\omega\epsilon |k_x|^2} |H_z|^2 (\gamma_g^2 k_x^*). \tag{42}$$

Following a similar procedure for LSE-modes, it is found that

$$S_x^\mu = \frac{1}{\omega\mu |k_x|^2} |E_z|^2 (\gamma_g^2 k_x^*). \tag{43}$$

References

[1] D. Phatak, N. D. Das, and A. P. Defonzo, "Dispersion characteristics of optically excited coplanar striplines: Comprehensive full-wave analysis," *IEEE Trans. Microwave Theory Tech.*, vol. 38, pp. 1719–1730, Nov. 1990.

[2] L. Carin and N. K. Das, "Leaky waves on broadside-coupled microstrip," *IEEE Trans. Microwave Theory Tech.*, vol. 40, pp. 58–66, Jan. 1992.

[3] R. Marqués, F. Mesa, and M. Horno, "On the correct expansion of leaky modes of planar transmission lines in surface-wave waveguide modes," in *Proc. 23rd European Microwave Conf.*, Madrid, Spain, Sept. 1993, pp. 432–434.

[4] R. E. Collin, *Field Theory of Guided Waves*, 2nd ed. New York: IEEE Press, 1991.
[5] L. B. Felsen and N. Marcuvitz, *Radiation and Scattering of Waves*. Englewood Cliffs, NJ: Prentice-Hall, 1973.
[6] J. Boukamp and R. H. Jansen, "Spectral domain investigation of surface wave excitation and radiation by microstrip lines and microstrip disk resonators," in *Proc. 13th European Microwave Conf.*, Sept. 1983, pp. 721–726.
[7] W. C. Chew, *Waves and Fields in Inhomogeneous Media*. New York: Van Nostrand Reinhold, 1990.
[8] T. Itoh, "Spectral domain immitance approach for dispersion characteristics of generalized printed transmission lines," *IEEE Trans. Microwave Theory Tech.*, vol. MTT-28, pp. 733–736, July 1980.
[9] R. Marqués and M. Horno, "Dyadic Green's function for microstrip-like transmission lines on a large class of anisotropic substrates," in *Proc. Inst. Elec. Eng.– Microwaves, Optics & Antennas*, pt. H, vol. 133, pp. 450–454, Dec. 1986.
[10] R. B. Adler, L. J. Chu, and R. M. Fano, *Electromagnetic Energy Transmission and Radiation*. Cambridge, MA: M.I.T. Press, 1969.
[11] C. M. Krowne, "Fourier transformed matrix method of finding propagation characteristics of complex anisotropic layered media," *IEEE Trans. Microwave Theory Tech.*, vol. MTT-32, pp. 1617–1625, Dec. 1984.
[12] N. K. Das and D. M. Pozar, "A generalized spectral-domain Green's function for multilayer dielectric substrates with application to multilayer transmission lines," *IEEE Trans. Microwave Theory Tech.*, vol. MTT-35, pp. 326–335, Mar. 1987.
[13] F. Mesa, R. Marqués, and M. Horno, "A general algorithm for computing the bidimensional spectral dyadic green's function: The Equivalent Boundary Method (EBM)," *IEEE Trans. Microwave Theory Tech.*, vol. 39, pp. 1640–1649, Sept. 1991.
[14] ——, "An efficient numerical spectral domain method to analyze a large class of nonreciprocal planar transmission lines," *IEEE Trans. Microwave Theory Tech.*, vol. 40, pp. 1630–1640, Aug. 1992.
[15] N. K. Das and D. M. Pozar, "Full-wave spectral-domain computation of material, radiation, and guided wave losses in infinite multilayered printed transmission lines," *IEEE Trans. Microwave Theory Tech.*, vol. 39, pp. 54–63, Jan. 1991.
[16] W. C. Chew and J. A. Kong, "Resonance of the axial-symmetric modes in microstrip disk resonators," *J. Math. Phys.*, vol. 21, no. 3, pp. 582–591, Mar. 1980.
[17] L. M. Delves and J. N. Lyness, "A numerical method for locating the zeros of an anlytic function," *Math. Comput.*, vol. 21, pp. 543–560, 1967.
[18] W. H. Press, B. P. Flannery, S. A. Teukolsky, and W. T. Vetterling, *Numerical Recipes: The Art of Scientific Computing (Fortran Version)*. New York: Cambridge Univ. Press, 1989.
[19] D. Nghiem, J. T. Williams, D. R. Jackson, and A. A. Oliner, "Leakage of the stripline dominant mode produced by a small air gap," in *Proc. IEEE MTT-S Dig.*, 1992, pp. 491–494.

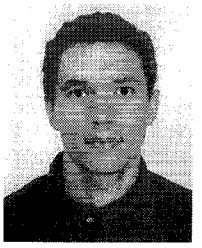

Francisco Mesa was born in Cádiz, Spain, on April 15, 1965. He received the Licenciado degree in June 1989 and the Doctor degree in December 1991, both in physics, from the University of Seville, Seville, Spain.

He is currently assistant professor in the Department of Applied Physics at the University of Seville. His research interests focus on electromagnetic propagation/radiation in planar lines with general anisotropic materials.

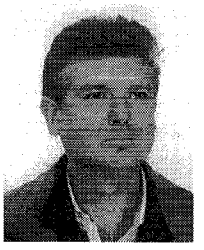

Ricardo Marqués was born in San Fernando, Cádiz, Spain. He received the degree of Licenciado in physics in June 1983, and the degree of Doctor in physics in July 1987, both from the University of Seville, Seville, Spain.

Since January 1984, he has been with the Department of Electronics and Electromagnetism at the University of Seville, where he is currently associate professor in electricity and magnetism. His main field of interest includes MIC devices design, wave propagation in anisotropic media, and electromagnetic theory.